Adhesion of vesicles to curved substrates

Sovan Das*
Department of Mathematics, Pennsylvania State University, University Park, Pennsylvania 16802, USA

Qiang Du†
Department of Mathematics and Department of Materials Science and Engineering, Pennsylvania State University, University Park, Pennsylvania 16802, USA

(Received 12 November 2007; published 15 January 2008)

We investigate the adhesion of vesicles, under the influence of a contact potential, to substrates with various geometry. For axisymmetric configurations, we find that the transition from a free vesicle to a bound state depends significantly on the substrate shape. In general, the critical values of the contact potential at which these transitions take place are lower for a concave-shaped substrate than that for a flat-shaped substrate investigated in earlier studies. We observe that the transitions happen at higher critical values of the contact potential when the substrate is convex and illustrate how these critical values depend on the curvature of the substrate. In addition, we construct an approximate analytical solution that predicts the shape of the vesicle for large internal excess pressure and contact potential. The analytical solution leads to an inequality that relates the surface tension with the contact potential.

DOI: 10.1103/PhysRevE.77.011907 PACS number(s): 87.16.D−, 82.70.Uv, 68.35.Np, 46.15.Ff

I. INTRODUCTION

Adhesion is a key mechanism for the survival of many cells and organism, and it occurs ubiquitously in nature. Biological processes such as endocytosis, exocytosis, cell crawling, and locomotion, through which a cell communicates with and responds to the surrounding environment, are influenced by adhesion [1]. Efficient drug delivery has enormous impact in biotechnology, and it crucially depends on adhesion of a vesicle membrane to a target plasma membrane. Biosensor applications also require binding of membrane to a substrate [2–5]. It is now established that stem cells differentiate into various cell types including neurons, myoblasts, and osteoblasts depending on the stiffness of the elastic substrate that they adhere to [6]. The cytoskeletal network within the cell provides the key mechanism for the adhesion to a substrate and senses the stiffness of the substrates [1,7,8]. Meanwhile, tissue or matrix microenvironments are known to influence adhesion and the cytoskeleton including cell shape and proliferation [1,8–13]. Moreover, investigations of adhesion and cell mechanics using techniques such as the atomic force microscopy (AFM) show that the mechanical properties of the cell membrane also play important roles [14].

In this work, we study the adhesion of giant unilamellar vesicles (GUVs) to elucidate the role of membranes played in adhesion. GUVs are lipid bilayer vesicles with sizes in the micrometer range and a few nanometers of thickness and can be treated as two-dimensional surfaces in a three-dimensional space [15]. Lipid bilayer vesicles are closed membranes that form spontaneously in an aqueous environment under suitable conditions and represent a simplest model for the cell membrane without the complexity of membrane-bound proteins [2]. They can be studied using a variety of experimental techniques [16–21]. The membranes are assumed to be laterally incompressible, with their shapes controlled mainly by the bending elastic energy. This is because the area compression modulus is much larger than the bending stiffness of the membranes [22–25].

Most of the existing theoretical studies of adhesion are for flat substrates [15,26–31]. However, in many applications, substrates are not planar, but rather spatially and/or chemically patterned [4,32]. Cells and liposomes for drug delivery and other biotechnology applications frequently encounter substrates that are not flat. Despite this, little theoretical investigation on vesicle or cell adhesion on patterned substrates exists. There have been studies on adhesion of supported membranes to a structured substrates [3,4] where the supported membranes are obtained by spreading bilayers on a substrate or by transferring lipid monolayers using a Langmuir-Blodgett technique [5].

Recently, Shi *et al.* [33,34] developed and investigated a two-dimensional model for vesicle adhesion. They considered the vesicle as a contour of constant length L and found that the force displacement relationship of the vesicle and the maximum pull-off force depend on the substrate shape. Other theoretical and experimental studies on curved substrates consider binding of a vesicle membrane to micro- or nanoparticles or colloids [35–39]. In these works, the substrate particles are spheres and the characteristic substrate radius is much smaller than the radii of the vesicles.

We hereby investigate the adhesion of a three-dimensional vesicle to curved substrates, where the curvature of the substrates is comparable to the curvature of the vesicles. We consider strongly adhering giant vesicles or cells. In such a regime, when the substrate is flat, the vesicle membrane is separated from the substrate by a layer of water or polymer of thickness of a few nanometers [3,5]. The typical size of a vesicle or a cell varies between 0.1 and a few hundred micrometers. Consequently, the interaction potential for the adhesion between the membrane and the substrate can be con-

*das@math.psu.edu
†qdu@math.psu.edu

sidered as a contact potential [5,26]. When the curvature of the substrate is comparable to the vesicle or cell size, this still remains the case. For weakly adhering vesicles or membranes, reflection interference contrast microscopy studies show that the separation distance is a few tens of nanometers or more [5]. Undulation forces due to thermal fluctuations of the bilayer can play an important role in controlling the adhesion in this regime [5]. Moreover, the interaction potential varies as a function of the distance between the membrane and the substrate. We do not consider this situation in our current study.

We focus on axisymmetric deformations of the vesicles when the substrate has either a concave or a convex spherical shape. In the limit when the contact potential and the internal excess pressure are large compared to the bending stiffness of the membranes, we carry out a boundary layer analysis of the adhered shapes. A similar analysis has been conducted for free vesicles with two coexisting fluid phases in [40,41]. When the pressure and the contact potential are not large, there are no analytical solutions for the shapes; we thus solve the equations numerically. The numerical solutions lead to a phase diagram for bound-unbound transitions. These transitions were first investigated by Seifert and Lipowsky [26] and, subsequently, by Seifert [27] for two-dimensional vesicles and by Smith *et al.* [29] in the study of the effect of pulling forces.

The analytical solution constructed here predicts that the shape of the vesicle is close to a truncated sphere (outer sphere), except in the region close to the contact point where the tangent angle and the meridional curvature change rapidly. The region of rapid change forms a boundary layer. An inequality is found to relate the radius of the outer sphere with the contact potential normalized by the pressure. This, in turn, relates the surface tension with the contact potential. The bound and unbound transitions that we obtain are qualitatively similar, for most part, to that discussed in [26]. We also find a few other transition lines. Moreover, we observe that the critical values of the contact potential at which these transitions occur depend strongly on the substrate radius and the type of substrate (i.e., concave or convex). The concave substrates exert influence in favor of bound states, whereas the convex ones exhibit higher values of contact potential for which first bound states are observed.

II. VESICLES UNDERGOING ADHESION

Figure 1 shows a schematic of the closed axisymmetric vesicle adhered to substrates that we consider in the present work. In this simple, but very useful model, the fluid membrane is in contact with a rigid substrate in the shape of a spherical cap. During adhesion, the membrane segment of a bound vesicle interacts with the substrate wall and can experience a variety of intramolecular forces. These interactions are modeled by an effective contact potential W [26].

For a laterally incompressible fluid bilayer, with inner and outer monolayers indistinguishable and the long axis of the lipid molecules oriented along the direction normal to the membrane surface, the bending free energy per unit area has the form $f_b = f_b(H^2, K)$, where $H=(c_1+c_2)/2$ and $K=c_1c_2$ are,

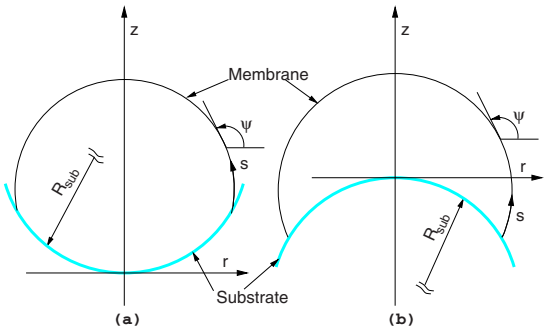

FIG. 1. (Color online) Schematic of adhered vesicles when the substrate is (a) concave and (b) convex. R_{sub} is the substrate radius, ψ is the tangent angle measured from horizontal, and s is the arclength measured from the contact point.

respectively, the mean and Gaussian curvatures of the membrane with c_1 and c_2 being the principal curvatures. One simple form of f_b is

$$f_b = \frac{\kappa}{2}(c_1 + c_2 - c_0)^2 + \kappa_g K = \frac{\kappa}{2}(2H - c_0)^2 + \kappa_g K, \quad (1)$$

where κ and κ_g are the bending stiffnesses corresponding to the mean and Gaussian curvatures, respectively, and c_0 is the spontaneous curvature [15,42–44]. This is the spontaneous curvature model. Other mechanical models that have been used to describe the shapes of vesicles and red blood cells are the bilayer couple model and the area difference elasticity model [45–48]. The total bending energy is obtained by integrating f_b over the entire membrane area. For a homogeneous vesicle with spherical topology, the integral of the Gaussian curvature is constant and the Gaussian curvature stiffness κ_g does not play a role. However, for a phase-separated membrane, κ_g does influence the shape through the jump conditions that relate the bulk equilibrium equations at the interface between the phases, provided it is different in the different phases [17,49]. For the current study we only consider zero spontaneous curvature ($c_0=0$).

With these, the free energy of the vesicle has the form

$$F = \int_\Gamma (2\kappa H^2 + \kappa_g K) d\Gamma - WA_c + \Sigma A + PV. \quad (2)$$

In the above, Γ denotes the free surface, A is the total surface area of the vesicle, V is the volume enclosed by the vesicle, A_c is the surface area of the vesicle that is in contact with the substrate, and Σ and P are the Lagrange multipliers for the area and volume constraints, respectively. If the volume of the vesicle is allowed to change by an osmotic pressure difference between the inside and outside of the vesicle, then P denotes this difference—i.e., $P=P_{ext}-P_{int}$. Similarly, when the area A is allowed to change, Σ denotes the surface tension in the membrane. Upon minimizing the free energy (2) we obtain the shape equation for the free surface of the vesicle. For an axisymmetric shape, the equation is

$$h'' + \frac{r'h'}{r} + 2h(h^2 - k) - \lambda h - \frac{p}{2} = 0, \tag{3}$$

where the prime denotes the derivative with respect to the arclength. When the lengths are made dimensionless by a linear size $\rho = \sqrt{A/4\pi}$, we obtain $h = \rho H$ and $k = \rho^2 K$. Also, $p = P\rho^3/\kappa$ and $\lambda = \Sigma\rho^2/\kappa$. Rescaling of lengths by ρ fixes the area to be 4π, and λ is determined as a Lagrange multiplier. Equation (3) is the same as the one obtained for a free vesicle without the adhesion [42,50] and with zero spontaneous curvature. The other equations obtained from the geometry of an axisymmetric deformation are

$$\psi' = 2h - \frac{\sin\psi}{r}, \quad r' = \cos\psi, \quad z' = \sin\psi. \tag{4}$$

The boundary condition at the line where the vesicle first makes contact with the substrate is given by $C_1^* = \sqrt{2W/\kappa} + C_w^*$, where C_1^* and C_w^* are the meridional curvatures of the vesicle and the substrates, respectively [26,51]. In the scaled mean curvature this condition becomes

$$h^* = \sqrt{\frac{w}{2}} + \frac{\sin\psi^*}{2r^*} + \frac{c_w^*}{2}, \tag{5}$$

with $w = W\rho^2/\kappa$ and $c_w^* = \rho C_w^*$. The quantities ψ^* and r^* are, respectively, the tangent angle and the distance from the axis of symmetry at the contact line. Note that the resistance to changes in the Gauss curvature κ_g does not appear in the boundary condition. If the vesicle remains intact, the tangent angle must be continuous at the contact line [26,51]. Then it can be shown that, due to the Gauss-Bonnet theorem, κ_g does not play a role because there is no discontinuity in the geodesic curvature of the membrane at the contact line [51]. The condition at the contact line for a more general form of the membrane free energy density and nonrigid substrates and a simple argument showing how the Gaussian curvature stiffness drops out of this condition can be found in [52]. The boundary conditions at the top $s = \hat{s}$, where $\hat{s}$ is an unknown parameter, are

$$\psi(\hat{s}) = \pi, \quad r(\hat{s}) = 0, \quad h'(\hat{s}) = 0. \tag{6}$$

As shown in Fig. 1, for a spherical substrate of radius R_{sub}, the boundary conditions at the line of contact, $s = 0$, are

$$\psi(0) = \psi^*, \quad r(0) \equiv r^* = \epsilon R_{sub}\sin\psi^*, \tag{7}$$

$$z(0) \equiv z^* = \epsilon R_{sub}(1 - \cos\psi^*), \tag{8}$$

and

$$h^* = \sqrt{\frac{w}{2}} + \epsilon\frac{1}{R_{sub}}, \tag{9}$$

where ϵ equals 1 for concave substrate and -1 for convex substrate. The quantity ψ^* is also an unknown parameter that we solve for, and $\hat{s}$ is determined from the area constraint

$$A_c + \int_0^{\hat{s}} 2\pi r ds = 4\pi,$$

where $A_c = 2\pi R_{sub}^2(1 - \cos\psi^*)$. In the following, we present a boundary layer analysis for the shape in the regime of large and negative (inner excess) pressure.

III. BOUNDARY LAYER ANALYSIS FOR THE SHAPE OF ADHERED VESICLES

When the dimensionless internal excess pressure and the contact potential are large—i.e., the bending effect is small—the overall vesicle shape is similar to the one given by the Laplace-Young equation for a soap film. This solution leads to a discontinuity in the tangent angle at the contact point which gives unbounded bending energy. For nonzero bending, this discontinuity is replaced by a region near the contact point where the curvature changes rapidly. This region gives rise to the boundary layer [53]. Boundary layer analyses for two-phase lipid vesicles are described in [40,41]. Here, we employ a similar approach.

We define a small parameter

$$\mu \equiv \sqrt{-2/p} = \sqrt{-2\kappa/(P\rho^3)}.$$

For μ small, Eq. (3) becomes

$$\mu^2\left(h'' + \frac{r'h'}{r}\right) + 2\mu^2 h(h^2 - k) - \tau h + 1 = 0,$$

where $\tau \equiv -2\lambda/p$. The other equations given in Eqs. (4) remain unchanged. In the following, we present the boundary layer analysis at the lowest order. As mentioned previously, w determines the curvature h at the contact point. When w is comparable to p, the mean curvature is large. Consequently, for the inner layer we scale s and h as

$$\xi = s/\mu, \quad h = \mathcal{H}/\mu.$$

Then ξ and $\mathcal{H}$ are, respectively, the stretched arclength and the scaled mean curvature. In terms of the scaled variables, the shape equations are

$$\ddot{\mathcal{H}} - \tau\mathcal{H} + 2\mathcal{H}^3 - 2\mu\mathcal{H}\frac{\sin\psi}{r}\left(2\mathcal{H} - \mu\frac{\sin\psi}{r}\right) + \mu\dot{\mathcal{H}}\frac{\cos\psi}{r} + \mu = 0, \quad \dot{\psi} = 2\mathcal{H} - \mu\frac{\sin\psi}{r}, \quad \dot{r} = \mu\cos\psi, \quad \dot{z} = \mu\sin\psi,$$

where the overdot denotes a derivative with respect to ξ. Due to the above scaling of h, to obtain the order-1 term in h in the inner layer, it is necessary to consider the equation for $\mathcal{H}$ at the order μ. Consequently, we expand $\mathcal{H}$ as $\mathcal{H} = \mathcal{H}_0 + \mu\mathcal{H}_1$ and $\tau = \tau_0 + \mu\tau_1$. It is not necessary to expand other variables to order μ [41]. The boundary conditions for $\mathcal{H}_0$ and $\mathcal{H}_1$ are obtained from Eq. (9) as

$$\mathcal{H}_0(0) = \sqrt{-w^*}, \quad \mathcal{H}_1(0) = \epsilon/R_{sub},$$

with $w^* = w/p$ and ϵ as defined earlier. The mean curvature h in the inner layer, up to order 1, is then given by (see [41] for details)

$$h = \frac{\sqrt{\tau_0}}{\mu}\,\mathrm{sech}\,\zeta + \left[T + \frac{2N}{r^*}\arctan(\sinh\zeta) + \frac{4M}{r^*}\ln(\mathrm{sech}\,\zeta)\right]\mathrm{sech}\,\zeta\tanh\zeta$$

$$-\frac{M}{r^*}\exp(-\zeta) + \frac{1}{\tau_0}(1-2\,\mathrm{sech}^2\zeta) + \left(\frac{3M}{r^*} + \frac{\tau_1}{2\sqrt{\tau_0}}\right)\mathrm{sech}\,\zeta(1-\zeta\tanh\zeta),$$

$$\psi = \psi^* + 2[\arctan(\sinh\zeta) - \arctan(\sinh\Upsilon)],$$

$$r = r^* = \epsilon R_{sub}\sin\psi^*, \quad z = \epsilon R_{sub}(1-\cos\psi^*),$$

where Υ and T are the undetermined constants for H_0 and H_1 which are to be determined from the corresponding boundary conditions $M=\cos[\psi^* - \arctan(\sinh\Upsilon)]/2$, $N=\sin[\psi^* - \arctan(\sinh\Upsilon)]$, and $\zeta=\sqrt{\tau_0}\xi+\Upsilon$. The quantity ψ^* is to be determined as well.

The outer solution is the one that describes the shape away from the contact point. In this region all the variables are order 1. However, to maintain consistency with the inner layer we take the expansion $\tau=\tau_0+\mu\tau_1$. The outer solution is given by a spherical cap of radius τ and at the lowest order:

$$h = \frac{1}{\tau_0}, \quad z = \hat{z} + \tau_0\left[\cos\left(\frac{\hat{s}-s}{\tau_0}\right) - 1\right],$$

$$\psi = \pi - \frac{\hat{s}-s}{\tau_0}, \quad r = \tau_0\sin\left(\frac{\hat{s}-s}{\tau_0}\right),$$

where $\hat{z}$ is the value of the height z at $s=\hat{s}$. Note that, at this point, the value of τ_1 does not appear at the lowest order. This implies that we cannot solve for τ_1 from this lowest-order analysis.

Next, we carry out an asymptotic matching of the outer and inner layer expressions. For asymptotic matching, we make the inner and outer solutions agree in an intermediate region [53]. To obtain expressions for the inner layer in an intermediate region, we let ξ go to ∞. After the substitution $s=\mu\xi$ the outer-layer solutions are expanded in powers of μ. The corresponding order-1 terms resulting from the inner and outer solutions are equated after taking the limits. The matching of h is identically satisfied, while the matching of ψ, r, and z and the conservation of total area give

$$\sinh\Upsilon = \tan\left(\frac{\psi^*}{2} + \frac{\hat{s}}{2\tau_0}\right), \tag{10}$$

$$\epsilon R_{sub}\sin\psi^* = \tau_0\sin\frac{\hat{s}}{\tau_0}, \tag{11}$$

$$\hat{z} + \tau_0\left(\cos\frac{\hat{s}}{\tau_0} - 1\right) = \epsilon R_{sub}(1-\cos\psi^*), \tag{12}$$

$$\tau_0^2\left(1-\cos\frac{\hat{s}}{\tau_0}\right) = 2 - R_{sub}^2(1-\cos\psi^*). \tag{13}$$

From the boundary condition for $\mathcal{H}_0$ we obtain

$$\mathrm{sech}\,\Upsilon = \sqrt{-w^*/\tau_0}. \tag{14}$$

Combining Eqs. (10) and (14) and, subsequently, using Eqs. (11) and (13), we get

$$\cos\left(\psi^* + \frac{\hat{s}}{\tau_0}\right) = -1 - \frac{2w^*}{\tau_0}.$$

This gives a bound for w^* as $-\tau_0 \le w^* \le 0$ or, equivalently,

$$2\lambda \ge w \ge 0,$$

which gives a relation between the surface tension and the contact potential for bound vesicles.

Obtaining an analytical solution for Eqs. (10)–(14) is difficult. We compute the numerical solutions for Υ, τ_0, ψ^*, $\hat{s}$, and $\hat{z}$ instead, using the MATLAB function FSOLVE.

Finally, the composite solution, valid in the entire region, is obtained via

$$\text{composite solution} = \text{inner} + \text{outer} - \text{matching}$$

and takes on the form

$$\psi = \frac{s-\hat{s}}{\tau_0} + 2\arctan(\sinh\zeta), \quad r = \tau_0\sin\left(\frac{\hat{s}-s}{\tau_0}\right),$$

$$z = \hat{z} + \tau_0\left[\cos\left(\frac{\hat{s}-s}{\tau_0}\right) - 1\right],$$

and the composite solution for h is given by the corresponding inner solution. The composite solutions at the lowest order for r and z are their corresponding outer-layer solutions. The vesicle shape determined from this solution resembles that for the outer. A discontinuity of the tangent angle at the contact point is observed; note, however, that this is not the case in the actual shape. To avoid this apparent contradiction, we carry out the boundary-layer analysis up to one higher order (i.e., order μ). The analysis follows straightforwardly from that given in [41] and is omitted here. In Fig. 2, we show the shapes of vesicles obtained from the boundary-layer analysis up to order μ, superimposed with numerical solutions. The parameter values used are given in the caption along with the value of the tangent angle ψ^* at the contact point, obtained analytically and numerically. The agreement between the numerical and analytical shapes is very good in all the cases.

When w is not large—i.e., order 1—h is also order 1 in the inner layer and the rescaling of h is not necessary. In that case, it can be shown, using asymptotic matching at the lowest order, that $\psi^*=0$. This implies $r^*=z^*=0$. Then the shape resembles a free sphere. Again using a numerical solution, we observe nonspherical bound shapes above a critical value of w. In the following, we describe bound shapes and the bound-unbound transition of shapes using numerical solutions when the pressure and the contact potential are not large compared to the bending stiffness of the vesicle. In this regime, the shape equations are analytically intractable.

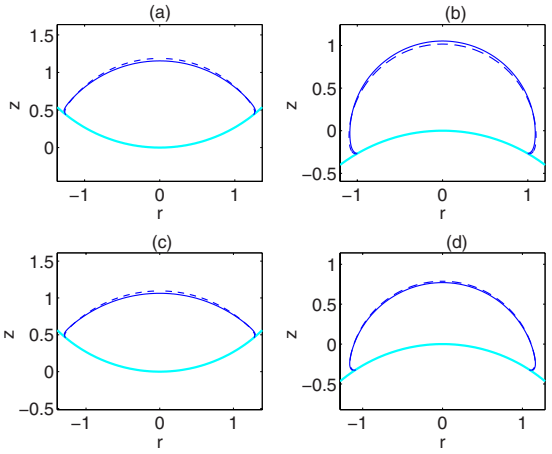

FIG. 2. (Color online) Comparison of analytical and numerical shapes of adhesion with $p=-800$, $R_{sub}=2$, and $w=600$ for (a) and (b) and $w=800$ for (c) and (d). The solid and dashed lines represent numerical and analytical shapes, respectively. Computed values of ψ^* (analytical, numerical) are (a) (0.6763, 0.6825), (b) (−0.5234, −0.5160), (c) (0.6944, 0.6991), and (d) (−0.5768, −0.5809).

IV. ADHERED SHAPES AND THEIR TRANSITIONS

We solve Eqs. (3) and (4) with boundary conditions (6)–(9) numerically using the MATLAB boundary value problem solver BVP4C. For free vesicles, the sphere is always a solution for any pressure p. However, nontrivial shapes arise as a result of bifurcation for $p=2l(l+1)$, where l is a positive integer larger than unity [43]. Some representative shapes, generated via numerical solution of the shape equations and adhered to the substrate, are shown in Fig. 3.

In the context of free vesicles, the shapes in Figs. 3(a) and 3(b) are oblate and they correspond to nontrivial solutions on the bifurcation branch at $p=12^+$. The shapes in Figs. 3(c) and 3(d) are nontrivial solutions for free vesicles on the bifurcation branch at $p=24^-$ [43]. We note that, due to a different scaling, the values of p in our study and those of [26] correspond to twice of those in [43].

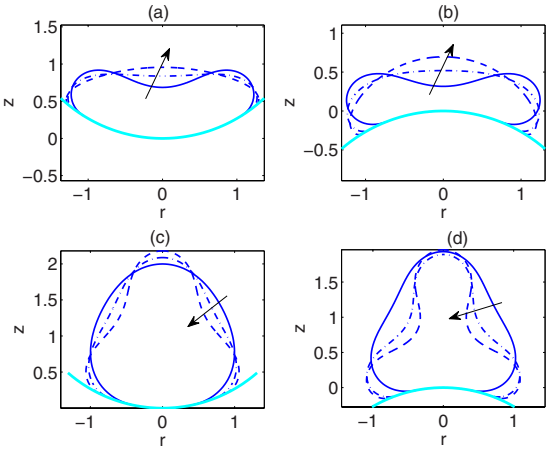

FIG. 3. (Color online) Some exemplary vesicle shapes for various values of w and $R_{sub}=2$. (a) Dimensionless volume $v=3$, (b) $v=2.5$, and (c) and (d) dimensionless pressure $p=22$. The arrow in each case indicates the direction of increasing w values.

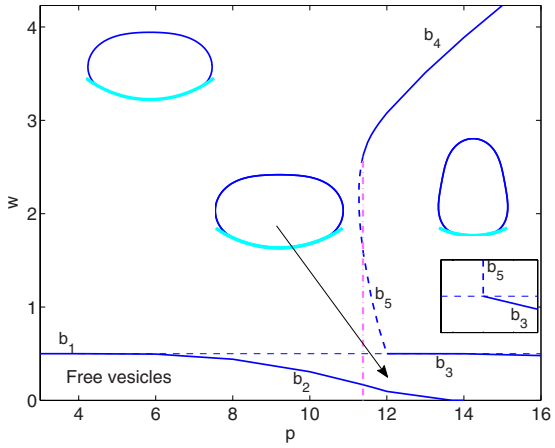

FIG. 4. (Color online) Bound-unbound transitions in the w-p parameter space for concave substrates of $R_{sub}=2$. Representative shapes are shown for each distinct region of the phase diagram. The plot in the inset is a close-up version around $p=12$ and $w=0.5$.

In Figs. 4 and 5 we present the phase behavior of the bound-unbound transition in the w-p parameter space for concave and convex substrates, respectively. The transition depends strongly on the type of substrate and the substrate radius. When the substrate is flat for $p<4$, a continuous transition occurs from bound state to free vesicle at $w=2$ [26]. For the adhesion of two-dimensional vesicles to a flat substrate Seifert [27] observed that at the critical transition value of w, the circle is a solution with $r^*=0$. In our study, we find that for $w=2(1-1/R_{sub})^2$ for concave substrates and $w=2(1+1/R_{sub})^2$ for convex substrates, with R_{sub} being the substrate radius, the unit sphere satisfies the boundary condition (5) with $r^*=0$. Thus the unit sphere is a solution to the shape equations and the boundary conditions and a continu-

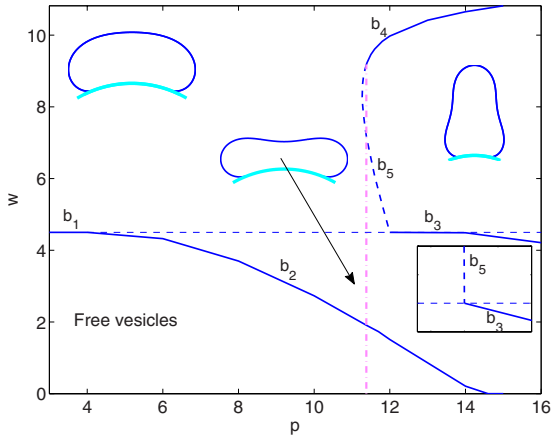

FIG. 5. (Color online) Bound-unbound transitions in the w-p parameter space for convex substrates of $R_{sub}=2$. Representative shapes are shown for each distinct region of the phase diagram. The plot in the inset is a close-up version around $p=12$ and $w=4.5$.

ous transition occurs from bound state to free vesicle for the above-mentioned values of w. We also verified these critical transition values using numerical solutions. This is also the case for all values of p larger than 4; however, a sphere does not give a shape with minimum energy, and other nonspherical shapes are realized.

Rewriting the critical transition value for convex substrates in terms of the quantities with dimension we get

$$W = \frac{2\kappa}{\rho^2}\left(1 + \frac{\rho}{\rho_{sub}}\right)^2 = 2\kappa\left(\frac{1}{\rho} + \frac{1}{\rho_{sub}}\right)^2, \tag{15}$$

where ρ is the linear size of the vesicle and ρ_{sub} is the substrate radius before scaling. When the vesicle is large compared to the substrate, ρ is significantly larger than ρ_{sub}; we obtain $W=2\kappa/\rho_{sub}^2$. That is, the contact potential exactly matches the bending energy density in the limit. This was observed earlier by Deserno [39] for a tensionless membrane binding to colloid particles.

The other transition lines do not follow such a simple relation. We obtain those using the numerical solutions of adhered shapes. The branch b_1 is for $p \leq 4$, and a continuous transition from bound vesicles to free spheres occurs when w crosses 0.5 for concave and 4.5 for convex substrates, respectively.

For $p > 4$, the horizontal dashed line denotes this transition. A discontinuous transition from bound to free oblate shapes occurs across branch b_2. Bound and free oblate vesicles coexist along this line. Bound prolate shapes exist and are stable in the region enclosed by the curves b_3, b_4, and b_5. Discontinuous transitions from bound prolate shapes to free prolate shapes and other bound shapes take place along these lines. However, the free prolate shapes along b_5 have higher energy than a free sphere.

The curves b_3 and b_5 meet at $(p,w)=(12,0.5)$ for concave substrates and $(12,4.5)$ for convex substrates (see the insets in Figs. 4 and 5). At this point, a continuous transition from bound prolate shapes to bound oblate shapes takes place as w is decreased and p is kept fixed at 12. Across the dash-dotted line at $p \approx 11.4$, a discontinuous transition from sphere to prolate shapes occurs for free vesicles. The curves b_1 and b_2 are similar to those observed by Seifert and Lipowsky [26] for flat substrates. We have also verified that the phase diagrams presented here look qualitatively similar for flat substrates, and we do not observe the branch D_a^{pr} for discontinuous transitions for the prolate shapes presented in Fig. 2 of [26]. The values of w at the transitions are, in general, larger for convex substrates than those for concave substrates for any specified p, which means that the concave substrates favor bound states, whereas convex ones are less favorable to adhesion.

When the substrate is axisymmetric but not spherical, the condition (5) at the contact line is still valid. The contact area A_c will have a form different from that mentioned for spherical substrates. The solution of the shape equations can be obtained in a way similar to that for spherical substrates. However, the stability of the solution can crucially depend on the substrate shape. For example, when the substrate is convex with a large curvature at the tip (e.g., a paraboloid), the contact potential required to bind to the tip will be large. It is more likely that the vesicle will break the symmetry and adhere to the side of the substrate away from the tip where it has smaller curvature. A situation like this cannot be investigated using an axisymmetric analysis. A spherical substrate has the same curvature everywhere, and this difficulty does not arise.

V. CONCLUSION

In this work, the adhesion of vesicles on curved substrates is studied. In the strong adhesion regime, with a contact potential, the substrate shape influences the critical values of the contact potential at which bound-unbound transitions occur. It is observed, in general, that concave substrates favor bound states more than convex substrates. This feature will allow the design of efficient manipulators of cells and liposomes. The strength of the vesicle and substrate interaction will determine the optimal shape for such manipulators. Conversely, a predetermined shape of the substrate will determine the optimal strength of the interaction. This, in turn, will determine the concentration and distribution of the adhesive elements on the substrate. We also obtain an approximate analytical solution for the bound vesicle shapes when the internal excess pressure and the contact potential are large compared to the bending stiffness of the membranes. In this regime, the shape is close to a spherical cap except in a small region near the contact line. The analytical solution delivers an inequality that relates the radius of the overall spherical shape and the ratio of the contact potential to pressure. We derive an equivalent inequality involving the surface tension and the contact potential.

Our current study is focused on the strong adhesion and axisymmetric geometry where the substrate is spherical. However, in real applications the situations can be different. In the weak adhesion regime fluctuations of the vesicle shape due to thermal excitation will play an important role. Then an entropic contribution to the free energy should be considered. This will increase the tendency of the vesicle to unbind [26]. An adhesion potential which is a function of the distance between the membrane and the substrate should be considered in such a case. Moreover, the substrate can have patterns that are not axisymmetric and the vesicle or cell can have nonaxisymmetric shapes. In our future work, we will address the distance-dependent adhesion potential by considering various forms of contact potential available in literature [27,30,54]. A more complex and nonaxisymmetric substrate geometry will also be considered via a phase field model previously developed for the study of free vesicle deformation [55–57].

ACKNOWLEDGMENTS

The authors would like to thank anonymous reviewers for valuable comments and suggestions to the discussion of axisymmetric nonspherical substrates. The research was supported in part by Grants Nos. NSF DMR-0205232, DMS 0712744, and NIH NCI 1R01CA125707-01A1.

[1] B. Alberts, A. Johnson, J. Lewis, M. Raff, K. Roberts, and P. Walter, *Molecular Biology of The Cell*, 4th ed. (Garland Science, New York, 2002).
[2] *Structure and Dynamics of Membranes*, edited by R. Lipowsky and E. Sackmann, Handbook of Biological Physics, Vol. 1 (Elsevier, Amsterdam, 1995).
[3] P. S. Swain and D. Andelman, Langmuir **15**, 8902 (1999).
[4] P. S. Swain and D. Andelman, Phys. Rev. E **63**, 051911 (2001).
[5] E. Sackmann, Science **271**, 43 (1996).
[6] A. J. Engler, S. Sen, H. L. Sweeney, and D. E. Discher, Cell **126**, 677 (2006).
[7] S. A. Safran, N. Gov, A. Nicolas, U. S. Schwarz, and T. Tlusty, Physica A **352**, 171 (2005).
[8] A. Nicolas, B. Geiger, and S. A. Safran, Proc. Natl. Acad. Sci. U.S.A. **101**, 12520 (2004).
[9] N. Q. Balaban, U. S. Schwarz, D. Riveline, P. Goichberg, G. Tzur, I. Sabanay, D. Mahalu, S. A. Safran, A. Bershadsky, L. Addadi, and B. Geiger, Nat. Cell Biol. **3**, 466 (2001).
[10] R. De, A. Zemel, and S. A. Safran, Nat. Phys. **3**, 655 (2007).
[11] A. Besser and S. A. Safran, Biophys. J. **90**, 3469 (2006).
[12] A. Nicolas and S. A. Safran, Biophys. J. **91**, 61 (2006).
[13] C. M. Lo, H. B. Wang, M. Dembo, and Y.-L. Wang, Biophys. J. **79**, 144 (2000).
[14] S. Sen, S. Subramanian, and D. E. Discher, Biophys. J. **89**, 3203 (2005).
[15] U. Seifert, Adv. Phys. **46**, 13 (1997).
[16] T. Baumgart, S. T. Hess, and W. W. Webb, Nature (London) **425**, 821 (2003).
[17] T. Baumgart, S. L. Das, W. W. Webb, and J. T. Jenkins, Biophys. J. **89**, 1067 (2005).
[18] J. T. Groves, Annu. Rev. Phys. Chem. **58**, 697 (2007).
[19] S. L. Veatch and S. L. Keller, Phys. Rev. Lett. **89**, 268101 (2002).
[20] S. L. Veatch and S. L. Keller, Biochim. Biophys. Acta **1746**, 172 (2005).
[21] S. L. Veatch and S. L. Keller, Biophys. J. **85**, 3074 (2003).
[22] E. A. Evans, Biophys. J. **30**, 265 (1980).
[23] H. P. Duwe, J. Käs, and E. Sackmann, J. Phys. (Paris) **51**, 945 (1990).
[24] S. Leibler, in *Statistical Mechanics of Membranes and Surfaces*, edited by D. Nelson, T. Piran, and S. Weinberg editors (Springer-Verlag, Berlin, 2004).
[25] R. Waugh and E. A. Evans, Biophys. J. **26**, 115 (1979).
[26] U. Seifert and R. Lipowsky, Phys. Rev. A **42**, 4768 (1990).
[27] U. Seifert, Phys. Rev. A **43**, 6803 (1991).
[28] U. Seifert and S. A. Langer, Biophys. Chem. **49**, 13 (1994).
[29] A.-S. Smith, E. Sackmann, and U. Seifert, Europhys. Lett. **64**, 281 (2003).
[30] I. Cantat, K. Kassner, and C. Misbah, Eur. Phys. J. E **10**, 175 (2003).
[31] D. Ni, H. Shi, and Y. Yin, Colloids Surf., B **46**, 162 (2005).
[32] S. Gillmor and P. Weiss (unpublished).
[33] W. Shi, X.-Q. Feng, and H. Gao, Mol. Cell. Biol. **3**, 121 (2006).
[34] W. Shi, X.-Q. Feng, and H. Gao, Acta Mech. Sin. **22**, 529 (2006).
[35] C. Dietrich, M. Anglova, and B. Pouligny, J. Phys. II **7**, 1651 (1997).
[36] R. Lipowsky and H.-G. Döbereiner, Europhys. Lett. **43**, 219 (1998).
[37] M. Deserno and W. M. Gelbart, J. Phys. Chem. B **106**, 5543 (2002).
[38] M. Deserno and T. Bickel, Europhys. Lett. **62**, 767 (2003).
[39] M. Deserno, Phys. Rev. E **69**, 031903 (2004).
[40] J.-M. Allain and M. BenAmar, Eur. Phys. J. E **20**, 409 (2006).
[41] S. L. Das and J. T. Jenkins, J. Fluid Mech. **597**, 429 (2008).
[42] W. Helfrich, Z. Naturforsch. C **28**, 693 (1973).
[43] J. T. Jenkins, J. Math. Biol. **4**, 149 (1976).
[44] O. Y. Zhong-Can, J. Liu, and Y. Xie, *Geometric Methods in the Elastic Theory of Membranes in Liquid Crystal Phases* (World Scientific, Singapore, 1999).
[45] H. G. Döbereiner, E. Evans, M. Kraus, U. Seifert, and M. Wortis, Phys. Rev. E **55**, 4458 (1997).
[46] M. Jaric, U. Seifert, W. Wintz, and M. Wortis, Phys. Rev. E **52**, 6623 (1995).
[47] G. Lim, M. Wortis, and R. Mukhopadhyay, Proc. Natl. Acad. Sci. U.S.A. **99**, 16766 (2002).
[48] L. Miao, U. Seifert, M. Wortis, and H-G. Döbereiner, Phys. Rev. E **49**, 5389 (1994).
[49] F. Jülicher and R. Lipowsky, Phys. Rev. E **53**, 2670 (1996).
[50] J. T. Jenkins, SIAM J. Appl. Math. **32**, 755 (1977).
[51] R. Capovilla and J. Guven, Phys. Rev. E **66**, 041604 (2002).
[52] M. Deserno, M. M. Müller, and J. Guven, Phys. Rev. E **76**, 011605 (2007).
[53] E. J. Hinch, *Perturbation Methods* (Cambridge University Press, Cambridge, UK, 1991).
[54] A. C. Balazs, J. Polym. Sci., Part B: Polym. Phys. **43**, 3357 (2005).
[55] Q. Du, C. Liu, and X. Wang, J. Comput. Phys. **198**, 450 (2004).
[56] Q. Du, C. Liu, and X. Wang, J. Comput. Phys. **212**, 757 (2006).
[57] J. Zhang, S. L. Das, and Q. Du (unpublished).